# Synergism in binary nanocrystal superlattices leads to enhanced p-type conductivity in self-assembled PbTe/$Ag_2Te$ thin films

JEFFREY J. URBAN[1]*, DMITRI V. TALAPIN[2], ELENA V. SHEVCHENKO[2], CHERIE R. KAGAN[1] AND CHRISTOPHER B. MURRAY[1]

[1]I.B.M. T. J. Watson Research Center, Nanoscale Materials and Devices Group, 1101 Kitchawan Road, Yorktown Heights, New York 10598, USA
[2]The Molecular Foundry, Lawrence Berkeley National Laboratory, Berkeley, California 94720, USA
*e-mail: urban@post.harvard.edu

Published online: 21 January 2007; doi:10.1038/nmat1826

**The ordered cocrystallization of nanoparticles into binary superlattices enables close contact of nanocrystals with distinct physical properties, providing a route to 'metamaterials' design. Here we present the first electronic measurements of multicomponent nanocrystal solids composed of PbTe and $Ag_2Te$, demonstrating synergistic effects leading to enhanced p-type conductivity. First, syntheses of size-tuneable PbTe and $Ag_2Te$ nanocrystals are presented, along with deposition as thin-film nanocrystal solids, whose electronic transport properties are characterized. Next, assembly of PbTe and $Ag_2Te$ nanocrystals into AB binary nanocrystal superlattices is demonstrated. Furthermore, binary composites of varying PbTe–$Ag_2Te$ stoichiometry (1:1 and 5:1) are prepared and electronically characterized. These composites show strongly enhanced (conductance ∼100-fold increased in 1:1 composites over the sum of individual conductances of single-component PbTe and $Ag_2Te$ films) p-type electronic conductivity. This observation, consistent with the role of $Ag_2Te$ as a p-type dopant in bulk PbTe, demonstrates that nanocrystals can behave as dopants in nanostructured assemblies.**

The modular design of multicomponent solids using micro[1]- or nanometre[2,3]-scale particles provides access to unique combinations of stoichiometry and symmetry not available in single-component bulk solids[4]. Precise assembly of nanocrystals with desired optical, electronic and magnetic properties into binary nanocrystal superlattices provides a route to metamaterials with potentially novel chemical or physical properties[2]. A diverse collection of these structures has been recently reported; however, it remains unknown whether these complex structural properties will translate into modified physical properties. This manuscript reports the first electronic studies of these binary nanocrystal systems, demonstrating synergistic effects in which the p-type conductance of the composite system exceeds the sum of the individual nanoparticle components.

One classic example of intentionally introducing nanometre-scale particles to modify the physical properties of a solid is semiconductor doping. This concept, central to solid-state device physics, has been exceptionally difficult to realize in nanocrystalline materials[5,6]. Despite great interest in nanocrystal doping, there have been few successful reports to date, which led to the hypothesis that 'self-purification' phenomena intrinsically limit the introduction of impurities into nanocrystals[5,6]. Recent theoretical and experimental works corroborate this view, showing that 'self-purification' mechanisms are energetically favourable over dopant incorporation, particularly for small nanocrystals[6]. Therefore, there exists a need for alternative approaches to nanocrystal doping. This manuscript develops an alternative to traditional nanocrystal doping—the use of nanoparticles themselves as dopants in a multicomponent nanocrystalline solid.

Binary nanocrystal superlattices offer the potential to design these nanostructured solids with programmable chemical and structural features. Furthermore, the presence of labile organic shells creates an additional opportunity—the evolution of material properties as a function of nanocrystal coupling can be investigated[7]. With chemical treatment, heating or other methods, we can study the properties of nanocrystal solids with weakly interacting elements and then densify the solid to explore the strong-coupling limit. Here we study the influence of nanocrystal–nanocrystal interactions by preparing binary nanocrystal superlattices of PbTe and $Ag_2Te$ and measuring how the electronic properties of these multicomponent solids develop after heating and chemical treatment. These results represent the first steps in the rational design of a nanocrystal superlattice for a targeted physical application.

The choice of nanocrystal components, PbTe and $Ag_2Te$, was motivated by the goal of constructing highly conductive, granular, p-type nanocrystal composites. This combination of material properties was intentionally selected to yield a material with high p-type electronic conductivity and low thermal conductivity, desirable traits for the p-type leg of a thermoelectric device. PbTe has the highest thermoelectric figure of merit (ZT) of any single-phase bulk solid from 550 to 700 K (ref. 8), the target range for many waste-heat-recovery applications. The complementary component ($Ag_2Te$) was chosen because it provides $Ag^+$, which is an effective p-type dopant for bulk PbTe (ref. 9), with much more rapid diffusion rates than other common choices such as $I_2$ or $K^+$ (ref. 10). Additional advantages of this design are the substantial increases in phonon scattering

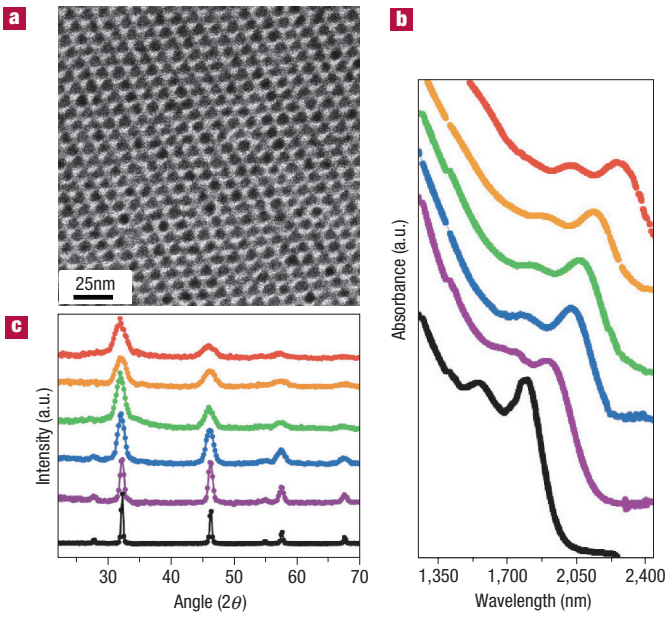


**Figure 1 Synthesis and characterization of PbTe nanocrystals. a**, TEM micrograph of 5.0 nm PbTe nanocrystals in a close-packed array. **b**, Series of optical absorption spectra obtained on 4.2, 5.5, 6.6, 7.5, 8.2 and 8.8 nm PbTe nanocrystals (from bottom to top). These spectra demonstrate the excellent mid-infrared tuneability of these PbTe nanocrystals. **c**, Series of XRD patterns obtained from 5.5, 6.2, 8.8, 10.5, 16.8 and 32.1 nm PbTe nanocrystals (from top to bottom). Analysis of peak width in each of these XRD patterns matches closely the diameters obtained for these samples from TEM.

inherent to nanocrystalline materials with high interface density[11,12] and known enhancements to the Seebeck coefficient in zero-dimensional materials[13]. Indeed, historical analysis of reported values of ZT illustrates that nanoscale patterning is essential to producing high-performance thermoelectric materials that exceed the $ZT = 1$ ceiling[14], as recent work on bulk solids with nanocrystal inclusions[15], Stranski–Krastanov dots in a bulk matrix of PbTe (ref. 13) and thin-film superlattice[16] materials has shown.

The PbTe nanocrystals synthesized for the binary composites (Fig. 1a) are size tuneable (~4–12 nm) and monodisperse (standard deviation ~ 5–6%) and form stable colloidal solutions as previously reported[17]. Changes in ligand concentration are used to control nanocrystal size by manipulating reaction kinetics via alterations in precursor stability. Structural information about nanocrystal composition, sizes and size distributions were obtained using several complementary techniques that access different length scales. Product composition, crystal structure and average crystallite size were obtained by analysing X-ray diffraction (XRD) patterns as shown in Fig. 1c. Nanocrystal diameters obtained from transmission electron microscopy (TEM) images (Fig. 1a) match those obtained from analysis of XRD patterns. Optical absorption of PbTe nanocrystal samples is also studied, as shown in Fig. 1b. This series of spectra shows that nanocrystalline PbTe samples possess tuneable, quantum-confined transitions (bulk PbTe has bandgap (measured at the band edge) 0.23 eV at 300 K) in the mid-infrared region. Additional details on the synthesis and characterization are available in the original reference[17].

Preparation of the $Ag_2Te$ nanocrystals necessary for the binary composites proceeds through a process of nanocrystal growth and subsequent ripening, phenomenologically similar to the digestive ripening of Au nanocrystals[18,19]. The evolution in $Ag_2Te$ nanocrystal size and shape is followed over a period of ~9 days by a combination of structural analysis (TEM, XRD and grazing-incidence small-angle X-ray scattering (GISAXS)) and optical spectra (near-infrared absorption), and is summarized chronologically in Fig. 2a–f. Figure 2a,d shows a TEM and optical spectrum corresponding to reaction products isolated ~1–5 h after injection of trioctylphosphine–tellurium complex (TOPTe). Here, the reaction contains a mixture of large (12–15 nm in diameter) and small (3–4 nm) $Ag_2Te$ nanocrystals, as shown in Fig. 2a. XRD analysis of reaction isolates confirms the orthorhombic $Ag_2Te$ structure (see Supplementary Information, Fig. S1). At this stage, there are two distinct features visible in the optical spectrum—one broad peak around ~1.15 μm and a sharp peak around ~1.4 μm. As this reaction is maintained at 85 °C it evolves as shown in Fig. 2b,e, which shows a TEM and optical spectrum obtained from reaction aliquots taken after ~3 days. The initial reaction has now evolved into a mixture of large, prolate crystals and small, spherical nanocrystals. The corresponding optical spectrum (Fig. 2e) shows an increase in the relative intensity and sharpness of the peak at ~1.15 μm. Subsequent aliquots from days 3–7 show a decrease in the amount of anisotropic species in solution, with a concomitant enrichment in the number of small, spherical $Ag_2Te$ nanocrystals. Whether this occurs owing to digestive ripening or the precipitation of insoluble, macroscopic chains of $Ag_2Te$ rods is now being explored. After maintaining the reaction for at least 8 days at 85 °C the solution consists entirely of monodisperse, spherical $Ag_2Te$ nanocrystals, as shown in Fig. 2c,f. Figure 2c demonstrates the excellent uniformity and monodispersity of the samples isolated at this stage. Optical absorption spectra now consist of a single, sharp feature at ~1.15 μm. Although these optical features are useful for monitoring reaction progress, their electronic origins are unknown at present, as $Ag_2Te$ is a relatively unexplored material. We note that the 1.15 μm peak is blue-shifted in a manner consistent with quantum-confined excitonic features (the bulk band-gap of $Ag_2Te$ is 0.064 eV (ref. 20)), although we have been unable to locate reliable reports of effective masses and dielectric constants of $Ag_2Te$ that would enable comparison of this assignment with simple Brus effective-mass calculations[21]. The evolution in particle shape and chaining of anisotropic $Ag_2Te$ particles are intriguing results we are now trying to better comprehend; however, for the assembly of binary nanocrystal superlattices, monodisperse, spherical particles are preferred, so we chose to focus on this element of the synthesis. Finally, the small $Ag_2Te$ crystals obtained by this method are monodisperse, and are used without further purification.

Formation of well-ordered nanocrystal solids requires building blocks with excellent uniformity. Therefore, we assemble thin nanocrystal films, not only anticipating future device studies, but also to confirm the high quality of the synthesis. Well-known self-organization processes associated with controlled solvent evaporation are exploited to produce highly ordered (structured over more than 100 particle diameters) nanocrystal thin solid films for characterization of their electronic properties. Owing to the hydrophobic character of the nanocrystal solutions, $SiO_2$ substrates are first pretreated with hexamethyldisilazane to ensure uniform wetting of the surface. After treatment, the nanocrystals are suspended in a hexane–octane solution (~8:1 by volume) and subsequently drop cast onto the $SiO_2$ surface. Analysis of the GISAXS, scanning electron microscopy (Supplementary Information, Fig. S2) and TEM images indicates the excellent spatial order (>10 μm per superlattice crystal in plane) of these polycrystalline superlattice films.

Having established preparative control over both PbTe and $Ag_2Te$ nanocrystal systems, we are now capable of designing artificial solids in which arbitrary nanocrystalline building blocks may be rationally cocrystallized into binary superlattices of desired

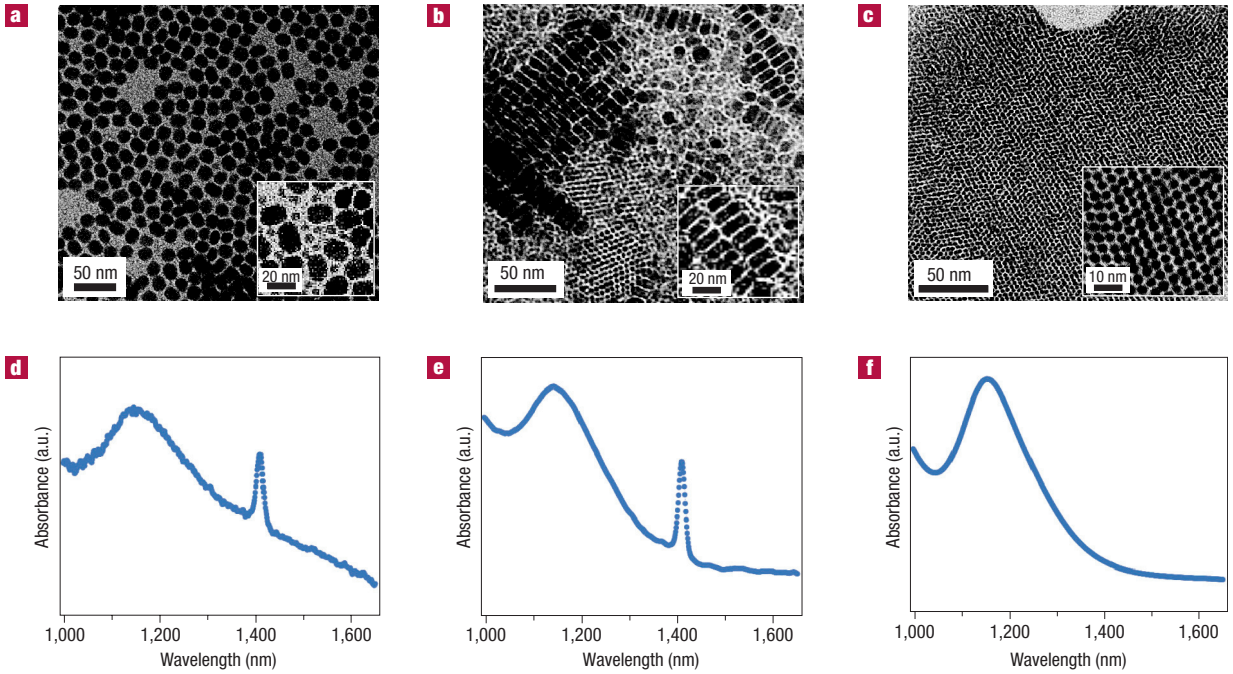


**Figure 2 Evolution of particle size and shape in $Ag_2Te$ nanocrystals.** **a**, TEM micrograph of $Ag_2Te$ nanocrystals isolated after 5 h of TOPTe injection. The inset shows that the reaction mixture contains both large (12–15 nm) and small (3–4 nm) nanocrystals at this stage. **b**, TEM micrograph of reaction products after ~3 days at 85 °C. The reaction mixture has evolved to contain both chains of large (>20 nm along the long axis) anisotropic particles and small (~3 nm) monodisperse crystals. The inset is a magnified portion of a TEM micrograph, highlighting the chaining process. **c**, TEM micrograph obtained from samples after 8 days reflux at 85 °C. The inset demonstrates the monodispersity of the crystals after more than 7 days. **d**, Optical absorption spectrum taken from 5 h reaction aliquot showing both a broad feature at ~1.15 μm and a sharp feature at ~1.4 μm. **e**, Optical absorption spectrum obtained from sample after ~3 days reflux. Here the ~1.15 μm peak has increased in intensity and sharpness relative to samples from the reaction mixture from less than 1 day. **f**, Optical absorption spectrum obtained from more-than-7-day samples. Only the ~1.15 μm absorption peak is present in the samples, corresponding to small, monodisperse nanocrystals.

stoichiometry and symmetry[2,4]. Here we report the assembly of binary AB superlattices[22] composed of PbTe and $Ag_2Te$ nanocrystals. Superlattice formation was pursued as a method to ensure the controlled patterning of both classes of nanocrystals, a design feature we wanted to use for the eventual design of bulk 'nanocrystalline solids' with programmed stoichiometry via sintering of these superlattice phases.

Assembly of binary nanocrystal superlattices by several groups[1–3] has highlighted three critical features necessary for formation: the relative size of each nanoparticle component, high monodispersity of each nanoparticle component and the ability to manipulate nanoparticle charge states. Both PbTe and $Ag_2Te$ are size tuneable and yield highly monodisperse nanocrystals, whose standard deviation is less than 5.5%. Also, reproducible superlattice samples (as judged by extent of superlattice formation, size of superlattice domains and lack of defects) were only achieved in samples in which small amounts (~10% by volume of a 1:100 dilute ligand/solvent mixture) of a charged amphiphilic ligand were added. These additives were included in an effort to narrow the charge-state distribution of individual nanocrystal populations, as discussed previously[2], although the charge distributions were not independently verified in this work.

Ordered binary nanocrystal superlattices (shown in Fig. 3a,b) are observed to form on slow evaporation of the solvent. Figure 3 highlights two different AB superlattice structures commonly observed: superlattices isostructural with NaCl (Fig. 3a) and CuAu (Fig. 3b). The assignment of these structures is based on analysis of two-dimensional Fourier transformation power spectra of real-space images (tilted along at least two principal axes) and consistency with three-dimensional lattice models built from the 180 most common crystallographic space groups using Accelrys MS Modelling 3.1 software. Also, owing to the size-tuneability of both nanocrystal systems, we have prepared both chemical isomers of these AB superlattices (that is, both PbTe (big)/$Ag_2Te$ (small) and PbTe (small)/$Ag_2Te$ (big) AB superlattices have been studied).

Previous work on nanocrystal transistors has demonstrated that the n-type transistor characteristics are far superior to the p-type characteristics, although less stable over time[23]. As such, our objective with the binary solids was to develop highly conductive p-type nanocrystal devices to complement this work. We targeted multicomponent composites composed of PbTe and $Ag_2Te$, because $Ag^+$ is an established p-type dopant for bulk PbTe[9,10]. In order to assess the doping efficacy of $Ag_2Te$ in the PbTe–$Ag_2Te$ composites, it is first necessary to fully characterize the electronic transport properties of PbTe and $Ag_2Te$ individually, and then compare these results to those obtained from composites. For this reason, we chose to first measure the electronic properties of each of the individual nanocrystal components in a thin-film transistor (TFT) measurement geometry.

Capturing the properties of nanocrystals in active solid-state devices is an appealing goal; however, there exist several challenges[23,24]: (1) the presence of bulky, insulating, ligand shells maintains large interparticle spacings and impedes electron transport, (2) surface dangling bonds create mid-gap trap states and (3) low dielectric constants result in charging energies greater than $k_BT$, where $k_B$ is the Boltzmann constant and $T$ the

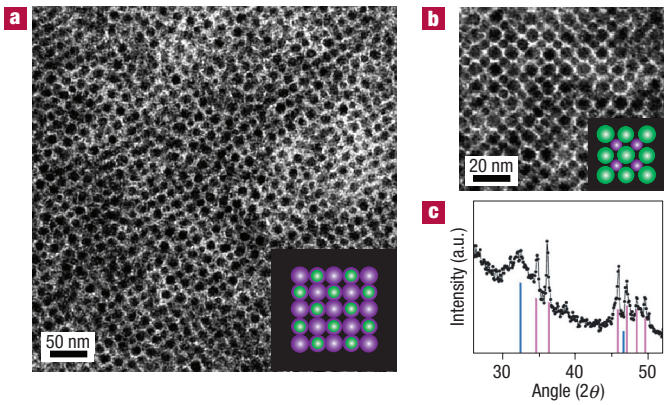


**Figure 3 Assembly of binary nanocrystal superlattices consisting of PbTe and $Ag_2Te$. a**, Superlattice assembled from 3.2 nm $Ag_2Te$ and 6.5 nm PbTe. The structure is consistent with a [100] projection of a NaCl lattice (inset). **b**, Superlattice assembled from 10.1 nm $Ag_2Te$ and 6.5 nm PbTe. This structure is consistent with a [100] projection of a CuAu lattice (inset). **c**, XRD of the solution used to make superlattice 3b deposited on a quartz plate. This XRD confirms the presence of both large $Ag_2Te$ and small PbTe components; the literature values for the $Ag_2Te$ and PbTe reflections are shown in magenta and blue, respectively.

temperature. Here we use the approach of chemical activation of nanocrystal solids by treatment with hydrazine[23], a chemical which decreases interparticle spacing by removing ligand shells while simultaneously passivating trap states. This activation process is carried out on both the PbTe and $Ag_2Te$ films, and increases their conductance dramatically (~10–11 orders of magnitude increase in conductance in PbTe; ~5–6 orders of magnitude enhancement in $Ag_2Te$).

Thin-film nanocrystal devices for electronic studies are prepared by depositing PbTe ($Ag_2Te$) nanocrystals from a hexane–octane solution onto highly doped silicon wafers with 100 nm $SiO_2$ thermal gate oxide and prepatterned source and drain Ti–Au (100/400 Å) electrodes (whose spacing was varied from 6 to 50 μm), as depicted in Fig. 4d. Although there are slight differences in processing between the TEM samples and the chips for transport measurements, the eventual removal of the ligands and evaporation of the solvent renders these changes insignificant. These films are characterized by GISAXS and scanning electron microscopy as discussed previously. Electronic measurements show that as-deposited films (PbTe or $Ag_2Te$) are insulating, demonstrate no gate effect and possess very low conductivities ($G \sim 10^{-13}$ S cm$^{-1}$), as shown in Supplementary Information, Fig. S3. At this stage, without hydrazine treatment, short (<3 h) thermal treatments up to 200 °C (under ambient pressure) do not dramatically enhance the conductance of the film (the best samples have $\sim G \sim 10^{-12}$ S cm$^{-1}$). Again, we attribute this poor conductivity to the small exchange coupling between nanoparticles arising from the large interparticle spacings maintained by the organic ligands. This perspective is supported by comparing GISAXS measurements of average interparticle spacings in single-component nanocrystal films before and after chemical activation (see Supplementary Information, Fig. S4). The data show that large enhancements in film conductivity (both PbTe and $Ag_2Te$) correlate directly to substantial decreases in average interparticle spacing (on average from ~1.7 to ~0.3 nm). Owing to the dramatic decrease in interparticle spacing, cracking often develops in the nanoparticle films after ligand removal, which necessitates multiple rounds of film deposition (on average three) to ensure a continuous film for transport measurements.

The chemical activation process involves treatment of the films with a 1.0 M solution of hydrazine in acetonitrile for 2–5 h, and subsequent washing with acetonitrile. After treatment, film conductivity is dramatically enhanced in both PbTe and $Ag_2Te$ films. For PbTe, initial hydrazine treatment results in ~10–11-order-of-magnitude enhancements in conductivity and gateable n-type behaviour as shown in Supplementary Information, Fig. S3. Immediately after hydrazine treatment, brief (<3 h) thermal treatments up to 150 °C (under ambient pressure) do not change the film conductance. However, as reported previously for PbSe transistors, prolonged heat treatment at higher temperatures desorbs hydrazine and ultimately switches device behaviour to p type, as shown in Fig. 4a,b. This process, and its effects on film transport, are reversible. Observing conventional TFT properties in the PbTe transistors enabled the calculation of linear-regime mobilities from these devices (n-type mobilities are ~0.95 cm$^2$ V$^{-1}$ s$^{-1}$; p-type mobilities are ~0.15 cm$^2$ V$^{-1}$ s$^{-1}$); a representative p-type gate scan is shown in Fig. 5b. All of the related data for the n-type PbTe transistors may be found in the Supplementary Information.

In contrast, although hydrazine treatment increases the conductivity of $Ag_2Te$ nanocrystalline films by ~5–6 orders of magnitude, it remains by comparison a very poor conductor and shows no discernible gate modulation of the current. The lack of conventional TFT device behaviour (either n or p type) in the $Ag_2Te$ films precludes the calculation of field-effect mobilities.

Assembly of PbTe–$Ag_2Te$ superlattices was pursued as a method of constructing highly conductive p-type nanocomposites of controlled composition. Ultimately, after sintering and ligand removal, these 'nanocrystal solids' would contain controlled quantities of electronic dopants homogeneously distributed throughout the solid, providing a method to circumvent common challenges associated with nanocrystal doping[5,6]. This concept motivated the incorporation of $Ag_2Te$ nanocrystals into the composites, as $Ag^+$ is an established p-type dopant for bulk PbTe with excellent mobility and low activation barriers for diffusion[9,10]. This alternative doping method was appealing, as traditional, direct substitutional approaches towards nanocrystal doping often result in exceptionally low, or zero, stable incorporation of dopants[5,6]. We report here the first electronic measurements on binary nanocrystal solids composed of PbTe and $Ag_2Te$. These initial measurements highlight the great potential for the 'nanoparticle as dopant' idea, showing substantial enhancements in conductivity compared to single-component PbTe or $Ag_2Te$ films. We present electronic measurements on nanocrystal films assembled with conditions and compositions consistent with formation of AB and $AB_5$ binary nanocrystal superlattices, referred to as 1:1 and 5:1 films, respectively. Ultimately, this procedure may allow exquisite control over both dopant concentration and doping profile by depositing films of binary nanocrystal superlattice crystals with desired stoichiometry and symmetry.

Preparation of the PbTe–$Ag_2Te$ nanocomposite films for measurement proceeds identically to the approach discussed for assembly of binary nanocrystal superlattices, except that a prepatterned silicon wafer is substituted for a TEM grid. These films are then immediately transferred to a nitrogen-filled dry-box and the electrical properties are characterized. As-deposited films are poorly conducting and show no gate effect (see Supplementary Information, Fig. S5), transmitting only ~pA or ~fA currents over 5–40 μm long channels ($G \sim 10^{-13}$ S cm$^{-1}$). As in the single-component film studies, we attribute these low conductivities to the bulky ligand shells. Without hydrazine treatment, short (<3 h) thermal treatments up to 200 °C (under ambient pressure) do not dramatically enhance the conductance of the film ($G \sim 10^{-12}$ S cm$^{-1}$). This is because large interparticle

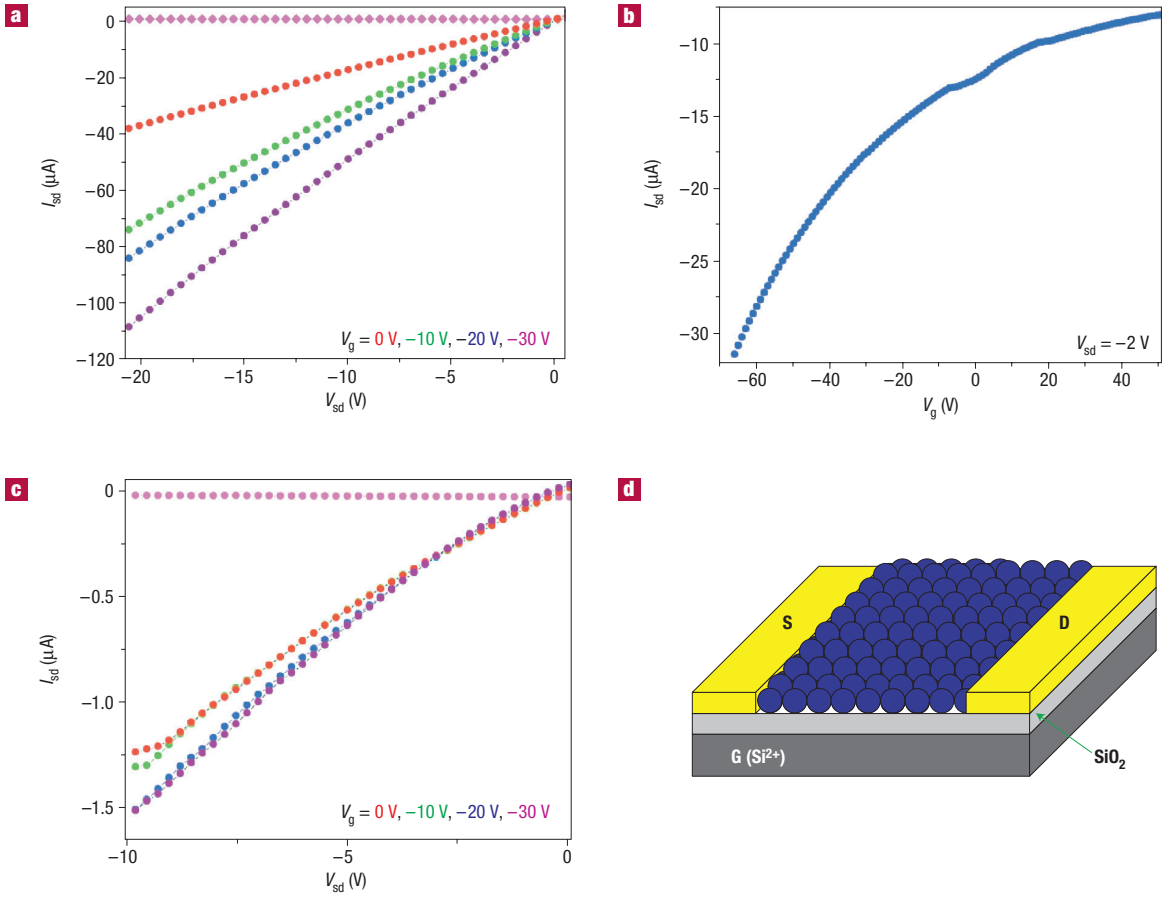


**Figure 4 Electronic characterization of single-component nanocrystal films.** All measurements were recorded in forward and reverse to assess device hysteresis. Gate currents (magenta) are also plotted to demonstrate that no current leakage occurs through the gate oxide. These gate currents ($I_g$) versus source–drain voltage ($V_{sd}$) are recorded in parallel for each source–drain current ($I_{sd}$) versus $V_{sd}$ measurement at every gate voltage; however, owing to the low $I_g$ values they seem collinear. **a**, $I$–$V$ measurement of p-type PbTe nanocrystal film in the linear regime. **b**, $I$–$V_g$ measurement of a PbTe nanocrystal film recorded with $V_{sd} = -2$ V, clearly demonstrating p-type behaviour. **c**, $I$–$V$ measurement of $Ag_2Te$ nanocrystal film. Even after chemical treatment, these films were poorly conducting and non-gateable, as shown by comparison of the −10 $V_g$ and −20 $V_g$ scans. **d**, Nanocrystal films were measured by deposition onto $Si/SiO_2$ wafers with prepatterned Ti–Au electrodes.

spacings are still maintained after heating, as thermogravimetric analysis shows that ligands are not decomposed until temperatures in excess of 400 °C (see Supplementary Information, Fig. S6). These high-temperature treatments are potentially destructive to the devices, and were not pursued.

As established previously, hydrazine treatment replaces the bulky capping groups and greatly decreases interparticle spacing. We used this approach here to bring the $Ag_2Te$ and PbTe nanocrystals into close contact. Immediately after treatment, large enhancements in electron transport were observed with average values of $G \sim 10^{-1}$ S cm$^{-1}$ for the most conductive 1:1 films. Owing to the larger lattice constant of binary nanocrystal superlattice systems relative to single-component lattices, we believe this enhanced conductance cannot be attributed only to decreases in interparticle spacing. Furthermore, the measured p-type behaviour in these systems, present even immediately after hydrazine treatment, indicates that the hydrazine itself is not the only operative mechanism.

Intriguingly, the best results were obtained by heating PbTe–$Ag_2Te$ nanocomposite samples previously treated with hydrazine (Fig. 5a,b) to 150 °C. As depicted in Fig. 5c, this mild heating does not seem to destroy superlattice order or cause nanoparticle melting. These samples subsequently show excellent hole transport with an averaged low-field conductance of $G \sim 0.35$ S cm$^{-1}$ and conductivities as great as $G \sim 4.8$ S cm$^{-1}$ for the most conductive 1:1 samples. As shown in Fig. 5a,b, the hydrazine-treated and heated composites show little gate modulation of their current, a result consistent with high carrier densities or homogeneous distribution of dopants. However, owing to the lack of an identifiable threshold voltage, standard analysis of the mobility and carrier concentration could not be executed here. We are now preparing samples for Hall effect measurements to quantitatively assess these parameters. For thermoelectric and power generation applications, however, we note that gating is irrelevant but that high electrical conductivity is imperative. Additionally, comparison of Fig. 5a,b with Fig. 4a,b reveals that the $I$–$V$ characteristics of the composite systems show nonlinear behaviour. These nonlinear features are consistent with electric-field-enhanced thermal activation of carriers from coulombic traps, as commonly seen in granular semiconducting systems[25]. However, despite these obvious similarities, further study is necessary to verify this hypothesis.

Although detailed studies of the mobility of each sample could not be carried out at this time, we did assess the efficacy of doping

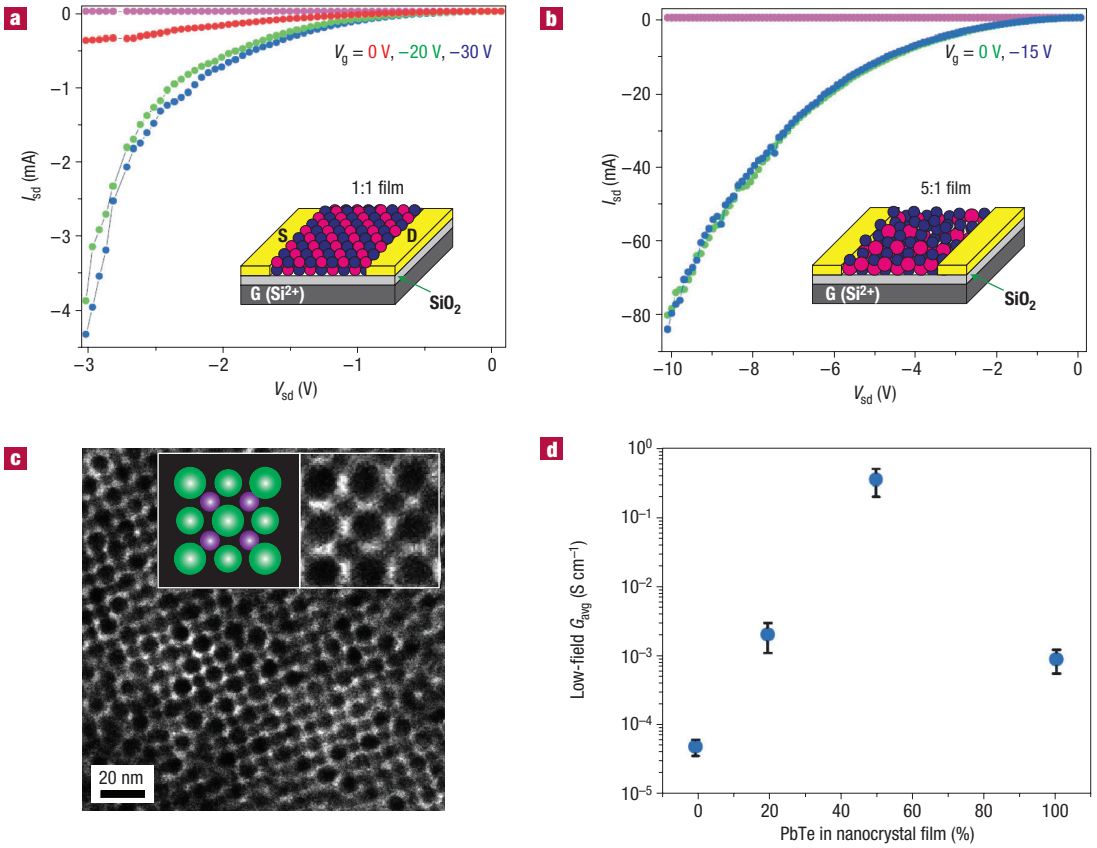


**Figure 5 Characterization of binary PbTe–$Ag_2Te$ nanocrystal films.** All measurements were recorded in forward and reverse to assess device hysteresis. Gate currents (magenta) are also plotted to demonstrate that no current leakage occurs through the gate oxide. These gate currents ($I_g$ versus $V_{sd}$) are recorded in parallel for each $I_{sd}$ versus $V_{sd}$ measurement at every gate voltage; however, owing to the low $I_g$ values they seem collinear. **a**, *I–V* measurement of 1:1 PbTe–$Ag_2Te$ binary nanocrystal film demonstrating high p-type conductivity and no gate response. **b**, *I–V* measurement of a 5:1 PbTe–$Ag_2Te$ binary nanocrystal film, again demonstrating p-type transport and no gate response. **c**, TEM micrograph of a 1:1 PbTe–$Ag_2Te$ superlattice after heat treatment, demonstrating that even 200 °C thermal treatments under vacuum do not abrogate superlattice order. **d**, Comparison of average low-field conductances (not exceeding 10 V in source–drain or 15 V in gate voltage) calculated over at least 12 devices for pure $Ag_2Te$ films, pure PbTe films, binary 1:1 PbTe–$Ag_2Te$ films and binary 5:1 PbTe–$Ag_2Te$ films. The average conductances for these compositions are $5.1 \times 10^{-5}$ S cm$^{-1}$, $9.21 \times 10^{-4}$ S cm$^{-1}$, 0.346 S cm$^{-1}$ and 0.0021 S cm$^{-1}$, respectively. The error bars are the standard deviations in conductance values for each of the compositions. These data demonstrate the synergistic enhancement of conductivity manifest in the binary nanocrystal solids.

by comparing the results for four different doping levels (Fig. 5d): pure PbTe, 5:1 (PbTe–$Ag_2Te$), 1:1 (PbTe–$Ag_2Te$) and pure $Ag_2Te$. These low-field conductances are compared under a consistent set of source–drain and gate voltages averaged over no fewer than a dozen devices. All other experimental parameters (oxide thickness, measurement geometry, contact materials) remained constant from sample to sample. The ratios of 1:1 and 5:1 were chosen because these are particle concentration ratios used to prepare AB and $AB_5$ binary nanocrystal superlattices. We note that, owing to the size of the devices created here (5,000 μm channel widths and 6–50 μm channel lengths) in comparison to average superlattice domain sizes (~2–4 μm$^2$), these measurements are recorded on polycrystalline binary nanoparticle systems. Although it is challenging to provide a direct correspondence between the formation of binary nanocrystal superlattices explored by microscopy and the electronic measurements provided here, this set of conditions was used as a guide for future experiments on coordinated structural and electronic measurements (see Supplementary Information, Fig. S7). Furthermore, structural studies indicate (Fig. 5c) that neither hydrazine nor thermal treatments materially disrupt the packing order present in both single-component and binary nanocrystal superlattices. As summarized in Fig. 5d, increased concentrations of $Ag_2Te$ in the binary composites result in enhanced conductivities, whereas the limiting cases of 100% PbTe and 100% $Ag_2Te$ possess the lowest conductivities. Based on previous experimental reports of conditions required for diffusion of $Ag^+$ into PbTe (refs 9, 10) and the established difficulty of aliovalent doping of nanostructures[5,6], we believe another mechanism is operative. Although distinct from conventional semiconductor doping processes, this approach has produced binary solids whose composite behaviour is enhanced over either of the individual components. Further studies are necessary to fully elucidate the mechanism of conductance enhancement, but this system bears similarity to reports of surface transfer doping[26] demonstrated in diamond[27] and silicon[28].

## METHODS

### NANOCRYSTAL SYNTHESIS AND ISOLATION

Synthesis of lead telluride nanocrystals proceeds according to the protocols developed in ref. 17.

Silver telluride nanocrystals are synthesized as follows: 0.091 g $AgNO_3$ (0.53 mmol) and 20 ml $H_2O$ are added to a flask containing 0.32 ml dodecanethiol (1.33 mmol) and 20 ml toluene. This mixture is stirred for 2–3 h to intermix the phases, after which stirring is stopped and the aqueous phase removed. The organic phase (containing both silver reagents and ligands) is then stirred and heated to 85 °C. Next, 3 ml of 0.75 M TOPTe is injected into the reaction mixture, which is subsequently maintained at 85 °C. After one day at 85 °C, a mixture of large (12–15 nm), prolate nanocrystals and small (4–5 nm), spherical nanocrystals is observed. Maintained at this temperature, the large, anisotropic nanocrystals stack together into chains (3–4 days) whereas the small nanocrystals develop into islands of monodisperse, spherical nanocrystals (7+ days). This synthesis has been carried out at several extended intervals from 7 to 12 days, and the reaction products do not change dramatically after ~9 days.

Isolation and purification of either PbTe or $Ag_2Te$ nanocrystals proceeds as outlined in ref. 17. Both classes of resulting nanocrystals are able to be resuspended in chloroform, hexane, tetrachloroethylene or several other solvents to form stable colloidal solutions.

### ASSEMBLY OF SINGLE-COMPONENT NANOCRYSTAL FILMS

Assembly of nanocrystal solids proceeds via controlled evaporation of a concentrated nanocrystal solution onto a substrate. Typical substrates are either Si–$SiO_2$ chips treated with hexamethyldisilazane at 150 °C for 30 min before nanocrystal deposition, silicon nitride membranes or amorphous-carbon-coated TEM grids. For electronic measurements of single-component nanocrystal solids, films were cast from a solution of PbTe ($Ag_2Te$) nanocrystals suspended in hexane–octane (~8:1 volumetric ratio). This produced films of excellent uniformity in both planar dimensions and thickness. Information on interparticle spacing and, more globally, the degree of ordering of the nanocrystalline films was obtained by GISAXS.

### ASSEMBLY OF BINARY NANOCRYSTAL SUPERLATTICES

Substrates are placed in a glass vial containing colloidal solutions of PbTe and $Ag_2Te$ nanocrystals (~10–50 μl of each component). The vial is tilted to a 60–70° angle and placed inside a low-pressure chamber maintained at 50 °C, as discussed previously[4]. Ordered binary assemblies form on controlled evaporation of the solvent. Preferred solvents are trichloroethylene, toluene or mixtures of both. Optimal superlattice formation (judged by length scale of ordering and defect density) is obtained by adding small amounts of either oleic acid or trioctylphosphine oxide solutions (~4 μl of 1:100 oleic acid–trichloroethylene by volume) to narrow the charge distributions of nanoparticle populations as discussed in ref. 2.

### SAMPLE CHARACTERIZATION

TEM, powder XRD, energy-dispersive X-ray spectroscopy and near-infrared absorption spectroscopy are used to characterize the size, shape, structure, composition and optical properties of the PbTe nanocrystals. Characterization of particle ordering and interparticle spacing in the PbTe films is carried out via GISAXS at grazing incidence using a D8 Discover series II diffractometer (Bruker) with a two-dimensional area detector. A copper anode was used as the radiation source (acceleration voltage 40 kV, flux 40 mA) and the signal integration time varied from 10 to 60 min. The angle of incidence was typically 0.83°, slightly greater than the critical angle of the nanocrystal film.

TEM and high-resolution TEM images were obtained using a Philips CM-12 microscope operating at 120 kV. Samples for TEM analysis were prepared by depositing a drop of dilute nanocrystal solution in chloroform or pentane on a 400 mesh carbon-coated copper grid and allowing the solvent to evaporate at room temperature. Statistical analysis of the size distributions of the nanocrystals is obtained using Scion Image data-processing software; for further details consult ref. 17.

Near-infrared absorption spectra were collected on trichloroethylene solutions of PbTe nanocrystals using a QualitySpec Pro infrared spectrometer (Analytical Spectral Devices). Wide-angle powder XRD measurements were carried out on a Bruker D500 diffractometer operating in the Bragg–Brentano configuration with Co K$\alpha$ radiation ($\lambda = 1.79$ Å) with scatter and diffraction slits of 1° and a 0.15 mm collection slit. Samples for wide-angle XRD measurements are prepared by depositing concentrated PbTe nanocrystal solutions in hexane onto a glass plate.

To study the electronic properties of nanocrystal assemblies (both single-component and binary assemblies) we deposited $40 \pm 10$ nm thick films of nanocrystals on 100 nm thick $SiO_2$ gate oxides thermally grown on heavily doped Si wafers used as the back gate. Source and drain Ti–Au (100/400 Å) electrodes were patterned on the $SiO_2$ surface by lithography before depositing the nanocrystal film. Spacing between the source and drain electrodes was typically 10 μm, that is, the typical path of charge carriers from source to drain electrode involved $\sim 10^3$ or more individual nanocrystals. Field-effect devices are tested using an Agilent 4156B semiconductor-parameter analyser. The source electrode was grounded. All room-temperature electrical measurements are carried out under dry nitrogen atmosphere.

Received 12 September 2006; accepted 12 December 2006; published 21 January 2007.

## References


1. Leunissen, M. E. *et al.* Ionic colloidal crystals of oppositely charged particles. *Nature* **437**, 235–240 (2005).
2. Shevchenko, E. V., Talapin, D. V., Kotov, N. A., O'Brien, S. & Murray, C. B. Structural diversity in binary nanoparticle superlattices. *Nature* **439**, 55–59 (2006).
3. Kalsin, A. M. *et al.* Electrostatic self-assembly of binary nanoparticle crystals with a diamond-like lattice. *Science* **312**, 420–424 (2006).
4. Shevchenko, E. V., Talapin, D. V., Murray, C. B. & O'Brien, S. Structural characterization of self-assembled multifunctional binary nanoparticle superlattices. *J. Am. Chem. Soc.* **128**, 3620–3637 (2006).
5. Erwin, S. C. *et al.* Doping semiconductor nanocrystals. *Nature* **436**, 91–94 (2005).
6. Dalpian, G. M. & Chelikowsky, J. R. Self-purification in semiconductor nanocrystals. *Phys. Rev. Lett.* **96**, 226802 (2006).
7. Koole, R., Liljeroth, P., de Mello Donega, C., Vanmaekelbergh, D. & Meijerink, A. Electronic coupling and exciton energy transfer in CdTe quantum-dot molecules. *J. Am. Chem. Soc.* **128**, 10436–10441 (2006).
8. Rowe, D. M. (ed.) in *CRC Handbook of Thermoelectrics* (CRC Press, New York, 1995).
9. Orihashi, M., Noda, Y., Kaibe, T. H. & Nishida, I. A. Evaluation of thermoelectric properties of impurity-doped PbTe. *J. Jpn Inst. Met.* **61**, 241–246 (1997).
10. Noda, Y., Orihashi, M. & Nishida, A. Thermoelectric properties of p-type lead telluride doped with silver or potassium. *J. Jpn Inst. Met.* **61**, 180–183 (1997).
11. Costescu, R. M., Cahill, D. G., Fabreguette, F. H., Sechrist, Z. A. & George, S. M. Ultra-low thermal conductivity in $W/Al_2O_3$ nanolaminates. *Science* **303**, 989–990 (2004).
12. Kim, W. *et al.* Thermal conductivity reduction and thermoelectric figure of merit increase by embedding nanoparticles in crystalline semiconductors. *Phys. Rev. Lett.* **96**, 045901 (2006).
13. Harman, T. C., Taylor, P. J., Walsh, M. P. & LaForge, B. E. Quantum dot superlattice thermoelectric materials and devices. *Science* **297**, 2229–2232 (2002).
14. Majumdar, A. Thermoelectricity in semiconductor nanostructures. *Science* **303**, 777–778 (2004).
15. Hsu, K. F. *et al.* Cubic $AgPb_mSbTe_{2+m}$ bulk thermoelectric materials with a high figure of merit. *Science* **303**, 818–821 (2004).
16. Venkatasubramanian, R., Siivola, E., Colpitts, T. & O'Quinn, B. Thin-film thermoelectric devices with high room-temperature figures of merit. *Nature* **413**, 597–602 (2001).
17. Urban, J. J., Talapin, D. V., Shevchenko, E. V. & Murray, C. B. Self-assembly of PbTe quantum dots into nanocrystal superlattices and glassy films. *J. Am. Chem. Soc.* **128**, 3248–3255 (2006).
18. Stoeva, S., Klabunde, K. J., Sorensen, C. M. & Dragieva, I. Gram-scale synthesis of monodisperse gold colloids by the solvated metal atom dispersion method and digestive ripening and their organization into two- and three-dimensional structures. *J. Am. Chem. Soc.* **124**, 2305–2311 (2002).
19. Lin, X. M., Jaeger, H. M., Sorensen, C. M. & Klabunde, K. J. Formation of long-range-ordered nanocrystal superlattices on silicon nitride substrates. *J. Phys. Chem. B* **105**, 3353–3357 (2001).
20. Dalven, R. Fundamental optical absorption in B-silver telluride. *Phys. Rev. Lett.* **16**, 311–312 (1966).
21. Brus, L. E. Electron–electron and electron–hole interactions in small semiconductor crystallites: The size dependence of the lowest excited electronic state. *J. Chem. Phys.* **80**, 4403–4409 (1984).
22. Saunders, A. E. & Korgel, B. A. Observation of an AB phase in bidisperse nanocrystal superlattices. *ChemPhysChem* **6**, 61–65 (2005).
23. Talapin, D. V. & Murray, C. B. PbSe nanocrystal solids for n- and p- channel thin film field-effect transistors. *Science* **310**, 86–89 (2005).
24. Yu, D., Wang, C., Wehrenberg, B. L. & Guyot-Sionnest, P. Variable range hopping mechanism in semiconductor nanocrystal solids. *Phys. Rev. Lett.* **92**, 216802 (2004).
25. Ben-Chorin, M., Moeller, F. & Koch, F. Nonlinear electrical transport in porous silicon. *Phys. Rev. B* **49**, 2981–2984 (1994).
26. Ristein, J. Surface transfer doping of semiconductors. *Science* **313**, 1057–1058 (2006).
27. Strobel, P., Riedel, M., Ristein, J. & Ley, L. Surface transfer doping of diamond. *Nature* **430**, 439–441 (2004).
28. Zhang, P. *et al.* Electronic transport in nanometre-scale silicon-on-insulator membranes. *Nature* **439**, 703–706 (2006).


## Acknowledgements

We gratefully thank the ONR (N00014-02-1-0867) for funding and support.
Correspondence and requests for materials should be addressed to J.J.U.
Supplementary Information accompanies this paper on www.nature.com/naturematerials.

## Author contributions

J.J.U. executed all of the materials syntheses, superlattice assembly, transport measurements and data analysis presented here. D.V.T. and E.V.S. provided general assistance and project suggestions. C.R.K. provided transport equipment and technical advice. C.B.M. provided general assistance, advice and project planning.

## Competing financial interests

The authors declare that they have no competing financial interests.